Journal of Power Sources 196 (2011) 8154–8159

Contents lists available at ScienceDirect

Journal of Power Sources

journal homepage: www.elsevier.com/locate/jpowsour

Synthesis of nano-Fe_3O_4-loaded tubular carbon nanofibers and their application as negative electrodes for Fe/air batteries

Akisuke Ito[a], Liwei Zhao[b], Shigeto Okada[b], Jun-ichi Yamaki[b,*]

[a] Interdisciplinary Graduate School of Engineering Sciences, Kyushu University, 6-1 Kasuga-Koen, Kasuga, Fukuoka 816-8580, Japan
[b] Institute for Materials Chemistry and Engineering, Kyushu University, 6-1 Kasuga-Koen, Kasuga, Fukuoka 816-8580, Japan

ARTICLE INFO

Article history:
Received 1 March 2011
Received in revised form 25 April 2011
Accepted 16 May 2011
Available online 27 May 2011

Keywords:
Fe_3O_4-loaded carbon materials
Negative electrode
Nano-carbon
Iron–air batteries

ABSTRACT

Nano-Fe_3O_4-loaded tubular carbon nanofibers (nano-Fe_3O_4/TCNFs) were synthesized by adding TCNFs into the high-temperature solution-phase reactions of iron(III) acetylacetonate with 1,2-hexadecanediol in the presence of oleic acid and oleylamine. The morphology and structure of this material were investigated by transmission electron microscopy (TEM) and X-ray diffraction (XRD) measurements. TEM observation clarified that nano-sized Fe_3O_4 particles with a uniform diameter of several nanometers were distributed and loaded tightly on the TCNF surfaces (inside and outside). After being annealed at 500 °C in Ar gas flow, nano-Fe_3O_4/TCNFs were used as the active material of negative electrodes for Fe/air batteries. Using an alkaline aqueous electrolyte with K_2S additive, a high specific capacity of 786 mAh g^{-1} and cycling efficiency of 76% at the 30th cycle were obtained. The downsizing of the conductive Fe_3O_4 nano-particles was considered to have contributed to the good electrochemical properties of the material.

1. Introduction

Rechargeable metal/air batteries are of special interest to battery researchers because they have much higher theoretical capacity than other sorts of batteries [1]. Metal/air batteries using several different metals have been investigated [2–5]. Among them, Fe/air batteries have received considerable attention due to their high theoretical capacity, long cycle life, high electrochemical stability, low cost, and environmental safety [6]. However, the practical application of Fe/air batteries has been limited by the thermodynamic instability of iron in alkaline environments and the low hydrogen overpotential of porous iron electrodes [7]. The hydrogen evolution reaction competes with the electrode discharge reaction and results in low battery cycling efficiency [8]. Various kinds of metal sulfide additives have been applied to iron electrodes [7,9–11] and/or associated electrolytes [9,10,12] to improve the electrochemical characteristics of Fe/air batteries. Our previous work demonstrated that the addition of carbon species into iron electrodes improved the conductivity and redox current [13]. Moreover, by loading Fe_2O_3 nanoparticles onto carbon nanotubes, the electrochemical characteristics of Fe/C electrodes were improved further [10,14,15]. However, these materials showed relatively high capacity at the initial several cycles, but their capacity faded after repeated cycling. Besides the effect of hydrogen evolution and the dissipation of soluble $HFeO_2^-$ species in the electrolyte during cycling, the large iron particle size (50 nm) and their poor dispersion on the carbon surface, which induced thick $Fe(OH)_2$ accumulation and high electrode resistance, should also take responsibility for the capacity fading. Therefore, iron oxide with smaller particles (a few nm) and better dispersion on the carbon surface (or better electrical conductivity) was expected to improve the electrochemical properties of an iron electrode in alkaline aqueous solutions.

Nano-sized magnetic iron oxide (Fe_3O_4) particles and their dispersions in various media have attracted the considerable interest of magnetic materials researchers [16,17]. Various kinds of synthetic methods have been developed to produce monodisperse nanoparticles with controlled size, shape, and composition due to their favorable characteristics. Among them, a simple organic-phase synthesis process was reported using iron(III) acetylacetonate as a precursor [18,19]. The monodisperse Fe_3O_4 particles could be controlled from 3 to 20 nm in diameter by simply varying the reaction temperature and the organic solvents. Although Fe_3O_4 nanoparticles have been widely used in magnetic nanodevices [20] and biomagnetic application [21–27], there have been few studies about the electrochemical properties of these monodisperse nanoparticles as an active material for batteries.

In the present study, Fe_3O_4 particles with diameters of several nanometers were loaded on the inside and outside surface of tubular carbon nanofibers (TCNFs) though a high-temperature

* Corresponding author. Tel.: +81 92 5837791; fax: +81 92 5837791.
E-mail address: yamaki@cm.kyushu-u.ac.jp (J.-i. Yamaki).

0378-7753/$ – see front matter © 2011 Elsevier B.V. All rights reserved.
doi:10.1016/j.jpowsour.2011.05.043

organic-phase reaction. After annealing, these nano-Fe_3O_4/TCNFs were used as the active material of negative electrodes for Fe/air batteries. The electrochemical properties were evaluated by charge/discharge measurements with and without K_2S as an additive in the alkaline aqueous electrolyte.

2. Experimental

The synthesis of nano-Fe_3O_4/TCNFs was carried out using standard commercially available reagents and lab-made TCNF. Iron(III) acetylacetonate ($Fe(acac)_3$, 99.9%), 1,2-hexadecanediol (90%), oleic acid (90%), and oleylamine (70%) were purchased from Sigma–Aldrich. Dibenzyl ether (97%) was from Wako Pure Chemical Co. TCNFs were lab-synthesized carbon nanotubes with an average diameter of ca. 50 nm [13]. Absolute ethanol and hexane (96%) were used as received without further purification.

The synthesis process was carried out in a three-neck flask at room temperature located on an orbital platform shaker (Rotamax 120, Heidolph). Iron(III) acetylacetonate (1 or 2 mmol) was ultrasonically dissolved in a mixture solvent consisted of oleic acid (3 mmol), oleylamine (6 mmol) and dibenzyl ether (10 ml) to obtain 0.1 mol dm^{-3} or 0.2 mol dm^{-3} $Fe(acac)_3$ solutions. Then TCNFs were ultrasonically dispersed in the solution with a certain iron-to-carbon weight ratio. For a 0.1 mol dm^{-3} $Fe(acac)_3$ solution, the ratio was controlled at 1:8. For 0.2 mol dm^{-3} $Fe(acac)_3$ solution, the ratio was controlled at 3:8. After 1,2-hexadecanediol (5 mmol) was added to the flask, the mixture was heated up to 200 °C at a heating rate of 10 °C min^{-1} under an Ar flow and kept at this temperature for 2 h, then heated further to reflux (300 °C) for 1 h. The resultant mixture was cooled to room temperature by removing the heat source. After adding excess hexane to the resultant mixture, the suspension was centrifuged to yield a black product. Then the product was washed in hexane and centrifuged several times. Finally, to remove organic residues from their surfaces, product particles were calcined for 3 h at 500 °C under Ar flow before undergoing electrochemical measurements.

The synthesized products were characterized by X-ray diffraction (RINT2100, Rigaku) with Cu Kα radiation (50 kV, 300 mA) from 2θ = 10–70° at a scan rate of 0.5° min^{-1}. The morphology and microstructure of the resulting particles were observed with transmission electron microscopy (TEM, JEM2100F, Jeol) by dropping the solution of the particles on carbon-coated copper grids.

To evaluate the electrochemical properties of the synthesized materials, electrochemical charge/discharge measurements were performed at 25 °C using a three-electrode glass cell. The working electrode was prepared by mixing 90 wt% synthesized materials and 10 wt% polytetrafluoroethylene (PTFE, Daikin Co.) and rolling. A SUS304 mesh was used as the current collector for the working electrode. A Pt mesh and Hg/HgO electrode (Inter Chemie Co.) were used as the counter electrode and the reference electrode, respectively. The electrolyte was an 8 mol dm^{-3} aqueous KOH solution with or without a 0.01-mol dm^{-3} K_2S additive. In the charging process, a galvanostatic charge step at a current density of 0.5 mA cm^{-2} was performed till −1.15 V, followed with a potentiostatic charge step. Simultaneously, a cut-off time was set for the whole charge process. The cut-off time were calculated by assuming the active material on the electrode had been fully charged at a constant current density of 0.5 mA cm^{-2}. The cutoff potential was set as −1.15 V because of the extensive hydrogen evolution observed at around −1.2 V. In discharging process, a galvanostatic step at a current density of 0.2 mA cm^{-2} was performed till −0.10 V. A relaxation period of 60 min was set at the end of each discharge/charge process. The discharge/charge capacities presented in the following discussion were obtained by integrating real current flow during cycling.

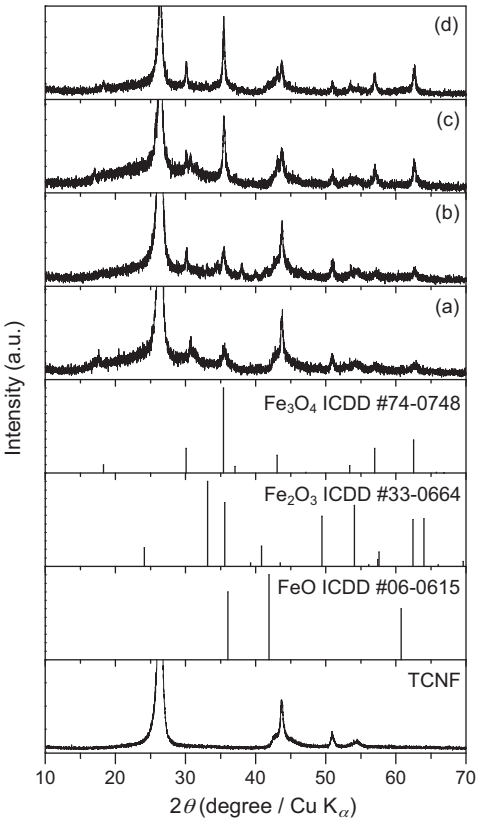

Fig. 1. X-ray pattern of nano-Fe_3O_4/TCNF (a) as-synthesized with 0.1 mol dm^{-3} $Fe(acac)_3$, (b) synthesized with 0.1 mol dm^{-3} $Fe(acac)_3$ followed by calcination, (c) as-synthesized with 0.2 mol dm^{-3} $Fe(acac)_3$, and (d) synthesized with 0.2 mol dm^{-3} $Fe(acac)_3$ followed by calcination.

3. Results and discussion

Fig. 1 shows X-ray diffraction patterns of the particles synthesized with different $Fe(acac)_3$ concentrations. With both 0.1 mol dm^{-3} and 0.2 mol dm^{-3} $Fe(acac)_3$, the successful synthesis of Fe_3O_4 particles was confirmed, although the TCNF signal overlapped with the XRD patterns of Fe_3O_4. Moreover, the synthesized nano-Fe_3O_4/TCNFs showed good resistance to high temperature up to 500 °C. After being calcined for 3 h at 500 °C under Ar flow, the nano-Fe_3O_4/TCNFs showed similar XRD patterns as that of the as-synthesized ones, with only a slight increase of the Fe_3O_4 signal. No identifiable XRD signals related to FeO or Fe_2O_3 were obtained. This indicated that no chemical reactions between carbon (TCNF) and Fe_3O_4 particles occurred, even at temperatures as high as 500 °C, in the Ar atmosphere.

TEM measurements were carried out in order to confirm the morphology of the Fe_3O_4 particles present on the TCNFs. Fig. 2 shows typical TEM images of the as-synthesized nano-Fe_3O_4/TCNF. The dark particles are Fe_3O_4 while the fibers are TCNFs. It was demonstrated that fine Fe_3O_4 particles dispersed on the TCNF surface. Moreover, synthesis conditions, including the concentration of $Fe(acac)_3$ and the iron-to-carbon ratio, had a direct effect on the particle size of Fe_3O_4. When $Fe(acac)_3$ was 0.1 mol dm^{-3} and the iron-to-carbon was 1:8, the particle size of Fe_3O_4 was around 8 nm except for a small amount of large particles. Most of the particles were well loaded on the surface of TCNF, both inside and outside. At the same time, some free Fe_3O_4 particles were found outside of TCNF. When the concentration of $Fe(acac)_3$ increased to 0.2 mol dm^{-3} and the iron-to-carbon was 3:8, the particle size increased to 10–20 nm, and the grain size distribution was much wider than that resulting from the 0.1 mol dm^{-3} $Fe(acac)_3$ condi-

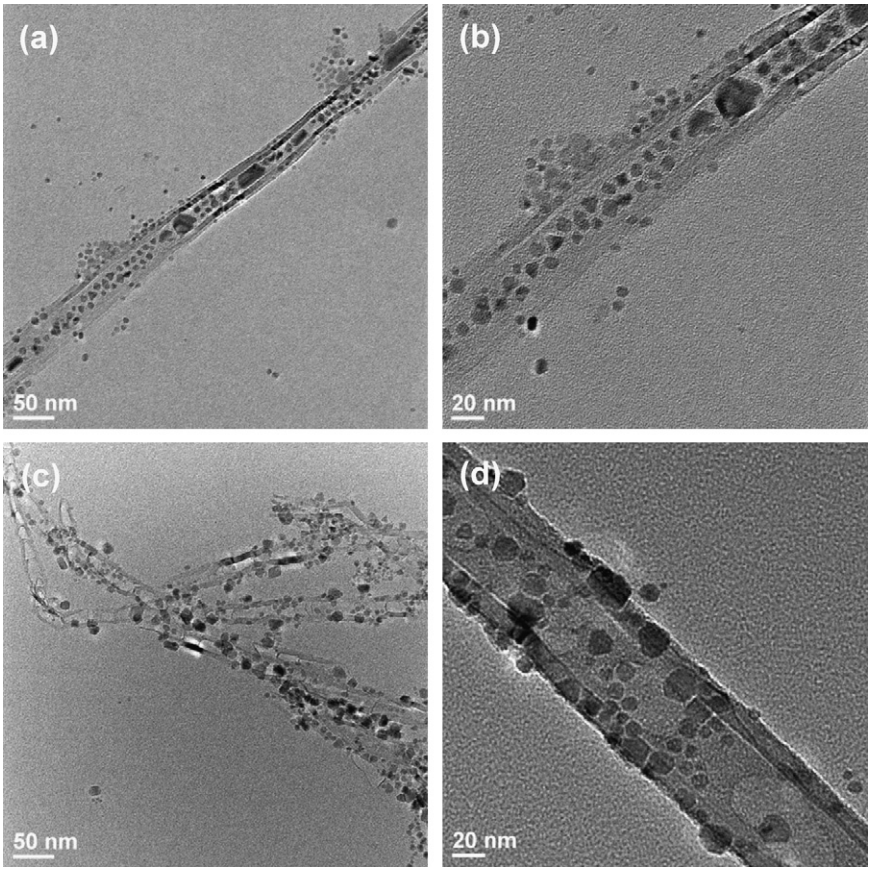

Fig. 2. TEM images of nano-Fe_3O_4/TCNF synthesized with (a and b) 0.1 mol dm^{-3} $Fe(acac)_3$ and (c and d) 0.2 mol dm^{-3} $Fe(acac)_3$.

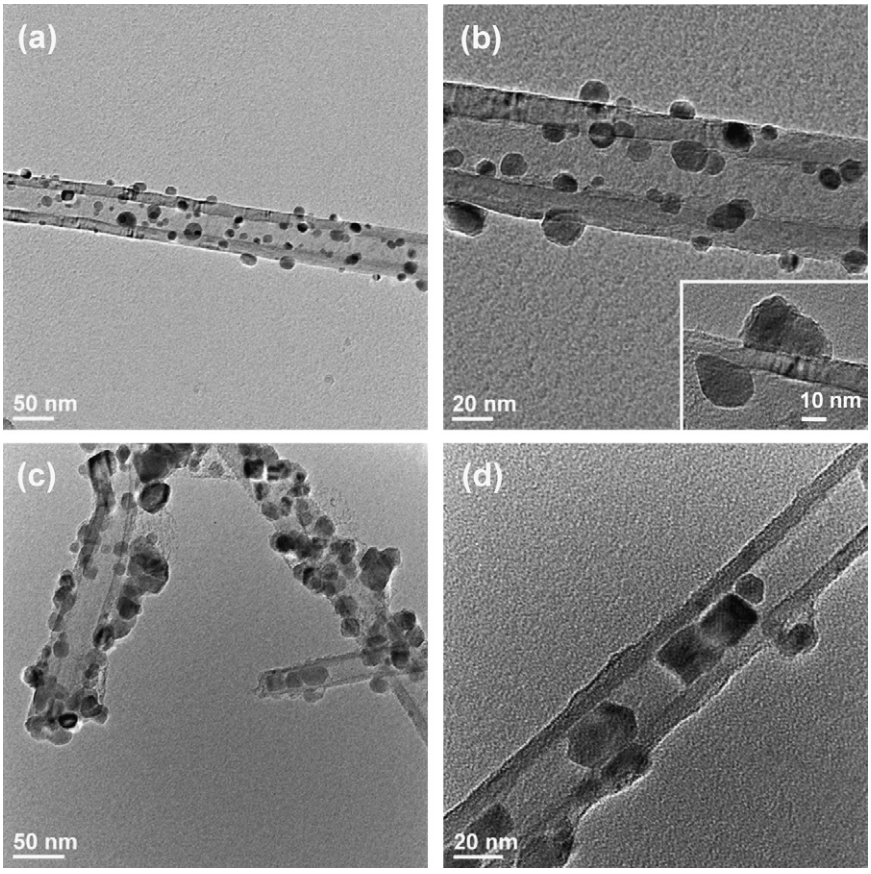

Fig. 3. TEM images of calcined nano-Fe_3O_4/TCNFs synthesized with (a and b) 0.1 mol dm^{-3} $Fe(acac)_3$ and (c and d) 0.2 mol dm^{-3} $Fe(acac)_3$.

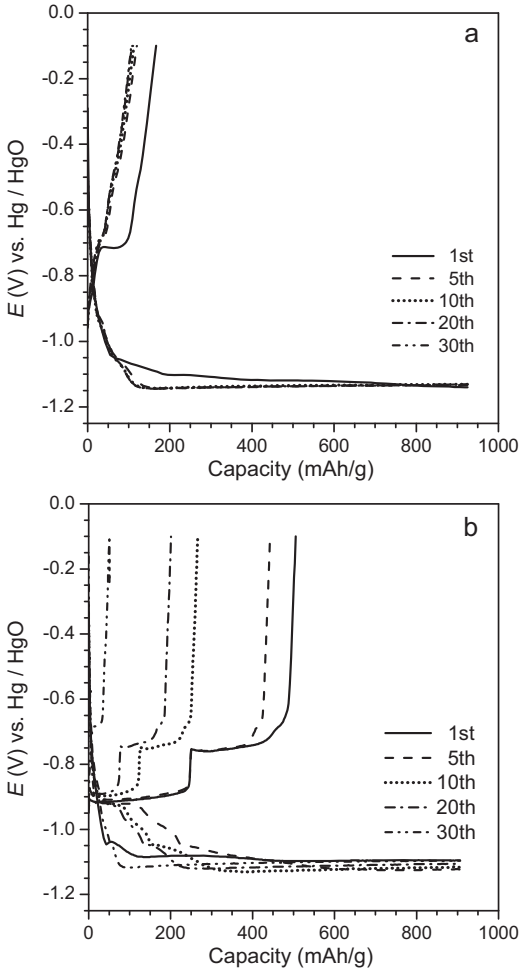

Fig. 4. The charge/discharge cycling profiles of nano-Fe_3O_4/TCNFs synthesized with (a) 0.1 mol dm^{-3} $Fe(acac)_3$ and (b) 0.2 mol dm^{-3} $Fe(acac)_3$.

tion. But almost no free Fe_3O_4 particles were found outside of TCNF, although the iron-to-carbon ratio was higher in this condition.

Normally, high temperature induces coalescence and sintering of nanoparticles. Therefore, the morphology of the calcined nano-Fe_3O_4/TCNFs was monitored by TEM to study their thermal stability. The images are shown in Fig. 3. Compared with that in as-synthesized materials, the Fe_3O_4 particles in the calcined nano-Fe_3O_4/TCNFs had a larger grain size. For the sample synthesized with 0.1 mol dm^{-3} $Fe(acac)_3$, the Fe_3O_4 particle size increased to 10–20 nm, but no remarkable degradation in the dispersibility of the Fe_3O_4 particles was observed. As for that synthesized with 0.2 mol dm^{-3} $Fe(acac)_3$, the Fe_3O_4 particle size increased to 20–40 nm, and the dispersibility of Fe_3O_4 particles worsened because of their large grain size. On the other hand, high temperature also showed a positive effect on the synthesized materials since the connection between the iron oxide particles and the carbon surface became stronger after heat treatment (see the inset of Fig. 3b).

The electrochemical properties of the nano-Fe_3O_4/TCNFs after heat treatment were evaluated by charge/discharge measurements. Fig. 4 shows the initial 30 charge (reduction of Fe_3O_4) and discharge (oxidation of Fe) curves of the nano-Fe_3O_4/TCNFs synthesized with 0.1 and 0.2 mol dm^{-3} $Fe(acac)_3$, respectively. The electrolyte used here was 8 mol dm^{-3} aqueous KOH solutions. For the sample synthesized with 0.1 mol dm^{-3} $Fe(acac)_3$, only a short plateau at about −0.72 V was observed in the first discharge curve, but this disappeared in the following cycles. The discharge capacity decreased from the initial 170 mAh g^{-1} to 100 mAh g^{-1} and remained at this level in the following cycles, although a charge capacity of 926 mAh g^{-1} was set for the electrode. The material synthesized with 0.2 mol dm^{-3} $Fe(acac)_3$ had different electrochemical characteristics, as shown in Fig. 4b. The initial discharge capacity was found to be 505 mAh g^{-1}, and two plateaus at about −0.92 and −0.72 V were observed in the first discharge curve. However, the discharge capacity faded rapidly in the following cycles, and only 50 mAh g^{-1} remained in the 30th cycle. From the discharge curves, it was easy to see that the capacity fading was mainly caused by the shortening of two plateaus, while the curve shape showed no significant difference. The electrochemical reactions of iron in alkaline solution have been reported as the following [28,29]:

$$Fe + 2OH^- \rightarrow Fe(OH)_2 + 2e^-, \quad E_0 = -0.975\,V \text{ vs.Hg/HgO} \qquad (1)$$

$$Fe(OH)_2 + OH^- \rightarrow FeOOH + H_2O + e^-, \; E_0 = -0.658\,V \text{ vs.Hg/HgO} \qquad (2)$$

and/or

$$3Fe(OH)_2 + 2OH^- \rightarrow Fe_3O_4{\cdot}4H_2O + 2e^-. \; E_0 = -0.758\,V \text{ vs.Hg/HgO} \qquad (3)$$

Theoretically, the plateau at −0.92 V should be attributed to Eq. (1) while the one at −0.72 V should be attributed to Eq. (3). And the reaction shown in Eq. (2) might be involved at the end of second plateau. However, as $Fe(OH)_2$ is a well-known insulater, the course of $Fe(OH)_2$ generation should be taken account into the reaction shown in Eq. (1). At the beginning of the discharge process, $Fe(OH)_2$ layer was formed and accumulated on the the surface of Fe particles gradually. Accordingly, a higher and higher overpotential was need for residual inner Fe to be oxidized to $Fe(OH)_2$. But when the potential increased to −0.75 V, the reaction shown in Eq. (3) started, which induced a gradual consumption of the $Fe(OH)_2$ layer. So it was supposed that a balance between these two reactions induced the long plateau at −0.72 V. It meant both reactions shown in Eqs. (1) and (3) might be involved in the second plateau at −0.72 V. Obviously, the short plateau appeared at the first discharge curve in Fig. 4a indicates a shallow reduction/oxidation process of Fe_3O_4 to $Fe(OH)_2$ during the first cycling, but no further processing to Fe occurred. The facts that no plateau was observed in the following cycles and the capacity was low implied that no reduction/oxidation of Fe_3O_4 occurred during further cycling. This meant that the nano-Fe_3O_4/TCNF synthesized with 0.1 mol dm^{-3} $Fe(acac)_3$ showed no electrochemical capability in alkaline solution. In the case of the nano-Fe_3O_4/TCNF synthesized with 0.2 mol dm^{-3} $Fe(acac)_3$, the appearance of two plateaus indicated the overall reduction/oxidation process of Fe_3O_4 to Fe. However, during further cycling, these two plateaus became short and induced capacity fading. This phenomenon indicated that the reduction/oxidation of iron in alkaline solution was gradually suppressed. Basically this phenomenon should be attributed to the evolution of hydrogen from the electrode.

To improve the electrochemical performance of nano-Fe_3O_4/TCNFs as the negative electrode of Fe/air batteries, 0.01 mol dm^{-3} K_2S was added to the alkaline electrolyte solution because K_2S has been proved to be an efficient additive in alkaline solutions to increase iron electrode capacity. Figs. 5 and 6 show the initial 30 charge/discharge curves and capacity retention of the nano-Fe_3O_4/TCNFs with K_2S as electrolyte additive. Obviously, the electrode capacity and cycling performance were improved greatly compared with that without the additive. For

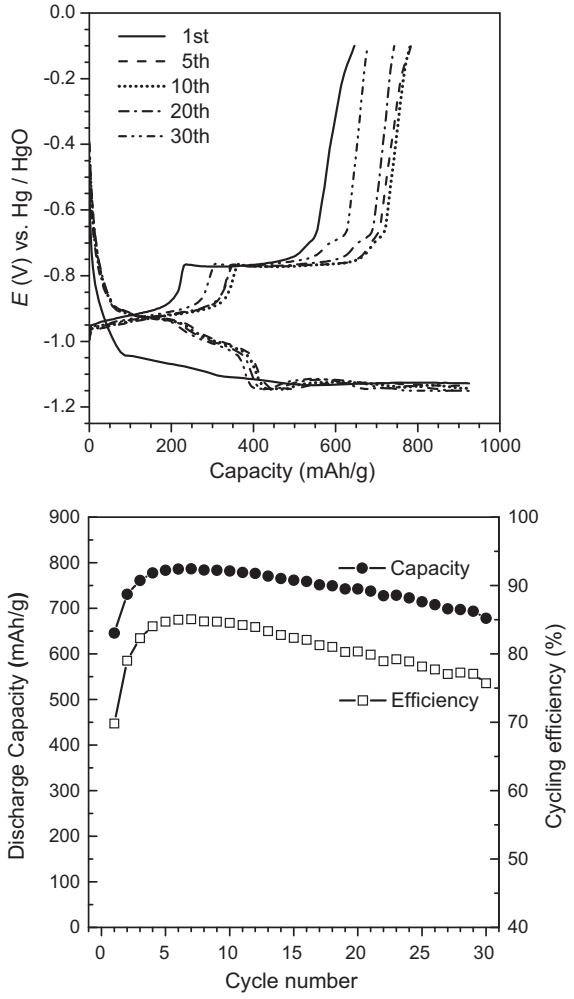

Fig. 5. The charge/discharge cycling profiles and capacity retention of nano-Fe_3O_4/TCNF synthesized with 0.1 mol dm^{-3} Fe(acac)$_3$ with K_2S electrolyte additive.

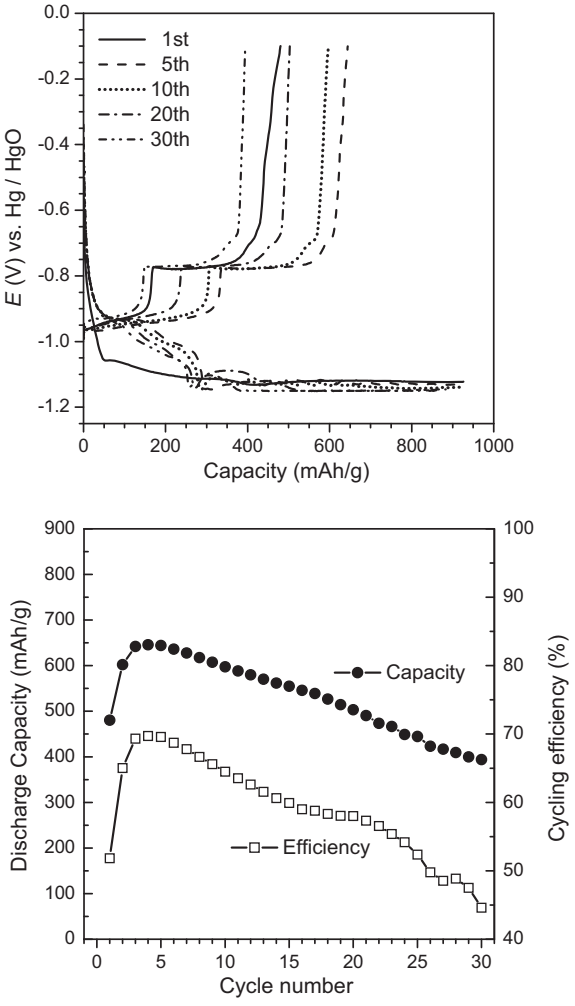

Fig. 6. The charge/discharge cycling profiles and capacity retention of nano-Fe_3O_4/TCNFs synthesized with 0.2 mol dm^{-3} Fe(acac)$_3$ using the K_2S-added electrolyte.

the sample synthesized with 0.1 mol dm^{-3} Fe(acac)$_3$, the initial discharge capacity was 646 mAh g^{-1}, and the maximum value was 786 mAh g^{-1} at the 7th cycle. Moreover, the capacity remained at about 676 mAh g^{-1} even after 30 cycles, which meant a good cycling performance. Besides, two stable plateaus at −0.77 V and −0.90 V in the discharged curves indicated steady reduction/oxidation reactions of iron during cycling. As for the sample synthesized with 0.2 mol dm^{-3} Fe(acac)$_3$, similar electrochemical behavior was obtained although the highest capacity was slightly lower, at 649 mAh g^{-1}, and the cycling efficiency decreased to 44% after 30 cycles. All these phenomena proved the excellent electrochemical characteristics of the nano-Fe_3O_4/TCNF composites with K_2S electrolyte additive, which were much better than those of the Fe_2O_3/TCNF composites in the same conditions [10]. The improvement might be attributed to the additional downsizing of active materials and the rather high conductivity of Fe_3O_4 [30,31]. The mean particle size of Fe_2O_3 in the Fe_2O_3/TCNF composites was 50 nm, which was larger than that of the Fe_3O_4/TCNF composites in the present study. Moreover, Fe_3O_4 is known as an iron oxide with rather high electrical conductivity, so the junction problem between the particles and carbons became nonsignificant, unlike that for the Fe_2O_3/TCNF composites [10,15]. On the other hand, comparing Figs. 5 and 6, obviously the nano-Fe_3O_4/TCNF synthesized with 0.1 mol dm^{-3} Fe(acac)$_3$ showed better electrochemical characteristics than that synthesized with 0.2 mol dm^{-3} Fe(acac)$_3$. This phenomenon also suggested the downsizing of the active materials to a few nm was effective at improving the electrochemical behavior of the iron electrodes in an alkaline aqueous solution.

When the alkaline solution was applied as an electrolyte in the Fe/air battery, hydrogen evolution (electrochemical reduction and subsequent desorption) was unavoidable during the electrochemical cycling even though the cut-off voltage was controlled at −1.15 V instead of −1.2 V in this work. Obviously, the hydrogen evolution was a competitive reaction in relation to the iron reduction/oxidation reactions. K_2S had been successfully applied as an electrolyte additive to suppress hydrogen evolution from the Fe/C mixed electrode of a Fe/air battery with alkaline electrolyte [9]. In this work, the application of K_2S was efficacious in improving the cycling performance of the nano-Fe_3O_4/TCNFs. Therefore, hydrogen evolution was deduced to be the main culprit for the capacity fading of the nano-Fe_3O_4/TCNFs in the alkaline electrolyte (Fig. 4). When hydrogen was generated and escaped from the electrode surface during cycling, Fe_3O_4 particles were peeled off from the surface of the TCNFs. This phenomenon caused the capacity fading. Because the Fe_3O_4 particles in nano-Fe_3O_4/TCNFs synthesized with 0.1 mol dm^{-3} Fe(acac)$_3$ were smaller than those synthesized with 0.2 mol dm^{-3} Fe(acac)$_3$, they were more easily peeled off from the TCNF surface (Fig. 4a). So a drastic capacity fading was obtained (Fig. 4a) with the nano-Fe_3O_4/TCNFs synthesized with 0.1 mol dm^{-3} Fe(acac)$_3$. In contrast, the nano-Fe_3O_4/TCNFs

synthesized with 0.2 mol dm^{-3} Fe(acac)$_3$ showed only gradual capacity fading (Fig. 4b). When K_2S was added into the alkaline electrolyte, the hydrogen evolution reaction was retarded by the sulfide ion. The S^{2-} additive was adsorbed at the electrode/electrolyte interface and then the molecular recombination reaction (step (III)) was inhibited by S^{2-} ion chemisorption [32]. Another possible reason is that the change in surface species in the K_2S-added electrolyte likely influences the overpotential of the hydrogen evolution reaction [33]. As the hydrogen evolution reaction was retarded, Fe_3O_4 particles could be kept on the TCNF surface more tightly, thereby improving the electrochemical properties of the nano-Fe_3O_4/TCNFs.

4. Conclusions

Nano-Fe_3O_4-loaded tubular carbon nanofibers (nano-Fe_3O_4/TCNF) were synthesized by a convenient process of adding the TCNF into organic-phase reactions of iron(III) acetylacetonate with 1,2-hexadecanediol in the presence of oleic acid and oleylamine. The Fe_3O_4 particles of several-nanometer diameters were dispersed and loaded tightly on the carbon surface. After being annealed at 500 °C in Ar flow, the nano-Fe_3O_4/TCNFs were applied as the active material of the negative electrode for Fe/air batteries. In an alkaline aqueous electrolyte with 0.01 mol dm^{-3} K_2S additive, a high specific capacity of 786 mAh g^{-1} and cycling efficiency of 76% at the 30th cycle were obtained. These properties were much better than those of the Fe_2O_3-loaded TCNFs prepared by aqueous-phase synthesis using iron nitrate hydrates. The downsizing of the conductive Fe_3O_4 nanoparticles was considered to have contributed to the good electrochemical properties of the material. Nano-Fe_3O_4/TCNF composites were found to be promising candidates for the active material in electrochemical devices.

Acknowledgements

The authors wish to express their thanks to Sumitomo Chemical Co., Ltd. for the support, to Prof. Seong-Ho Yoon (Institute for Material Chemistry and Engineering, Kyushu University, Japan) for providing the TCNFs for this study.

References

[1] D. Linden, T.B. Reddy, Handbook of Batteries, third ed., McGraw-Hill, New York, 2002.
[2] K.F. Blurton, A.F. Sammells, J. Power Sources 4 (1979) 263.
[3] X.X. Zeng, J.M. Wang, Q.L. Wang, D.S. Kong, H.B. Shao, J.Q. Zhang, C.N. Cao, Mater. Chem. Phys. 121 (2010) 459.
[4] T. Wang, M. Kaempgen, P. Nopphawan, G. Wee, S. Mhaisalkar, M. Srinivasan, J. Power Sources 195 (2010) 4350.
[5] U. Casellato, N. Comisso, G. Mengoli, Electrochim. Acta 51 (2006) 5669.
[6] S.V. Falk, A.J. Salking, Alkaline Storage Batteries, vol. 1, Wiley, New York, 1969.
[7] T.S. Balasubramanian, A.K. Shukla, J. Power Sources 41 (1993) 99.
[8] N. Jayalakshmi, V.S. Muralidharan, J. Power Sources 32 (1990) 277.
[9] B.T. Hang, T. Watanabe, M. Egashira, I. Watanabe, S. Okada, J. Yamaki, J. Power Sources 155 (2006) 461.
[10] B.T. Hang, S.-H. Yoon, H. Okada, J. Yamaki, J. Power Sources 168 (2007) 522.
[11] C.A. Caldas, M.C. Lopes, I.A. Carlos, J. Power Sources 74 (1998) 108.
[12] J. Cerny, K. Micka, J. Power Sources 25 (1989) 111.
[13] B.T. Hang, M. Egashira, I. Watanabe, S. Okada, J. Yamaki, S.-H. Yoon, I. Mochida, J. Power Sources 143 (2005) 256.
[14] B.T. Hang, T. Watanabe, M. Egashira, S. Okada, J. Yamaki, S. Hata, S.-H. Yoon, I. Mochida, J. Power Sources 150 (2005) 261.
[15] B.T. Hang, H. Hayashi, S.-H. Yoon, S. Okada, J. Yamaki, J. Power Sources 178 (2008) 393.
[16] J. Park, K.J. An, Y.S. Hwang, J.G. Park, H.J. Noh, J.Y. Kim, J.H. Park, N.M. Hwang, T. Hyeon, Nat. Mater. 3 (2004) 891.
[17] F.X. Redl, C.T. Black, G.C. Papaefthymiou, R.L. Sandstorm, M. Yin, H. Zeng, C.B. Murray, S.P. O'Brien, J. Am. Chem. Soc. 126 (2004) 14583.
[18] S. Sun, H. Zeng, J. Am. Chem. Soc. 124 (2002) 8204.
[19] S. Sun, H. Zeng, D.B. Robinson, S. Raoux, P.M. Rice, S.X. Wang, G. Li, J. Am. Chem. Soc. 126 (2004) 273.
[20] K. Raj, R. Moskowitz, J. Magn. Magn. Mater. 85 (1990) 233.
[21] P. Oswald, O. Clement, C. Chambon, E. Schouman-Claeys, G. Frija, Magn. Reson. Imaging 15 (1997) 1025.
[22] R. Hergt, W. Andra, C.G. d'Ambly, I. Hilger, W.A. Kaiser, U. Richter, H.-G. Schmidt, IEEE Trans. Magn. 34 (1998) 3745.
[23] A. Jordan, R. Scholz, P. Wust, H. Fähling, R. Felix, J. Magn. Magn. Mater. 201 (1999) 413.
[24] D.K. Kim, Y. Zhang, J. Kehr, T. Klason, B. Bjelke, M. Muhammed, J. Magn. Magn. Mater. 225 (2001) 256.
[25] Q.A. Pankhurst, J. Connolly, J. Dobson, J. Phys. D: Appl. Phys. 36 (2003) R167.
[26] P. Tartaj, M.P. Morales, S. Veintemillas-Verdaguer, T. González-Carreño, C.J. Serna, J. Phys. D: Appl. Phys. 36 (2003) R182.
[27] C.C. Berry, A.S.G. Curtis, J. Phys. D: Appl. Phys. 36 (2003) R198.
[28] K. Micka, Z. Zabransky, J. Power Sources 19 (1987) 315.
[29] C. Chakkaravarthy, P. Periasamy, S. Jegannathan, K.I. Vasu, J. Power Sources 35 (1991) 21.
[30] N.N. Greenwood, A. Earnshaw, Chemistry of the Elements, first ed., Pergamon, Oxford, 1984.
[31] M.M. Thackeray, W.I.F. David, J.B. Goodenough, Mater. Res. Bull. 17 (1982) 785.
[32] R. Carta, S. Dernini, A.M. Polcaro, P.F. Ricci, G. Tola, J. Electroanal. Chem. 257 (1988) 257.
[33] R.S. Schrebler-Guzman, J.R. Viche, A.J. Arvia, Electrochim. Acta 24 (1979) 395.